Int. J. Electrochem. Sci., 16 **(2021)** 151047, doi: 10.20964/2021.01.75

International Journal of
ELECTROCHEMICAL
SCIENCE
www.electrochemsci.org

Core-shell Fluorine-silicon Modified Polyacrylic Coating for Corrosion Protection of 304 Stainless Steel Substrate

Xia Wang[*], *Linglong Xu, Hui Wang, Xiong Li,Qiao Zhang,Yue Gu*

School of New Energy and Materials, Southwest Petroleum University, Chengdu, 610500, China
[*]E-mail: swpi_wx@126.com (Xia Wang), 1067206436@qq.com (Linglong Xu)

Received: 9 October 2020 / *Accepted:* 15 November 2020 / *Published:* 30 November 2020

A serious of core-shell fluorine-silicon modified polyacrylic emulsion had been prepared by seeded emulsion polymerization. Methylmethacrylate (MMA), butyl acrylate (BA) and acrylic acid (AA) were used as the monomers of polyacrylic core. And the shell of the emulsion was modified by polyacrylic with dodecafluoroheptyl methacrylate (DFMA), vinyl triethoxysilane (VTEO) and tetraethyl orthosilicate (TEOS). The completed of reaction was proved by fourier transform infrared spectroscopies (FT-IR). TEM analysis indicated core-shell structure of the hybrid particles. The surface analysis indicated that the excessive addition of VTEO-TEOS had a negative effect for the film. Electrochemical Impedance Spectroscopy (EIS) indicated that the anti-corrosion of the film went up first and then down with the increase of VTEO-TEOS content. The best anti-corrosion content of VTEO-TEOS was 1.0% (F-1.0Si). In this, the corrosion current density of the coating had reached $3.7\times10^{-8}A\cdot cm^{-2}$, the efficiency of anti-corrosion was 99.53%, the water contact angle was 99° and the thermal decomposition temperature was 298℃. Two glass transition temperature indicated that the emulsion was the structure of two phases with different properties. The high-efficiency anti-corrosion time of film within 300 h was showed with immersion experiment.

Keywords: Core-shell; Anti-corrosion; Stainless steel;Fluorine-silicon;Water diffusion

1. INTRODUCTION

As the strong strength, mechanical properties and hot workability, stainless steel had become one of widely used steel. Not only the stainless steel is used for and transportation industrial machines, but also for household products, auto parts, building materials and so on [1-4]. In order to maintain high-performance corrosion resistance, stainless steel needs to be surface cleaned. It's even worse than ordinary carbon steel while exposed to salty environment, especially in marine environment. Chloride corrosion is the most common degradation form of stainless steel, so, carbon steel needs to be cleaned frequently or coated with a protective film in heavily polluted or corroded areas [5,6]. Polyacrylate

emulsions and water dispersions are film-forming materials for waterborne acrylic coatings with high weather resistance and chemical resistance. The coating is a kind of green water-based coating with non-toxic and non-polluting[7,8]. However, there are still many problems in applying water-based polyacrylic coatings to the corrosion protection, such as poor crosslinking, general compactness, bad wettability and so on[9]. Physical and chemical modification with resins containing other special functional groups is a common way to improve performance of polyacrylic emulsion. Chemical modification increase the crosslinking of coatings, and physical blending is another way to improve coating performance by adding nanoparticles [10,11].

As the development of new emulsion polymerization and synthesis technology, the filmof polyacrylate coating has been greatly improved. Scholars had done a lot of research, but their directions of research mostly focused on the polymerization process or performance, few on the application of emulsions with special processes such as core-shell polymerization. Zhang et al. [12]prepared a core-shell self-crosslinking polyacrylate emulsion by semi-continuous seed emulsion polymerization. The effect of monomer content, neutralizer and curing temperature on emulsion crosslinking was studied. Emre et al. [13] synthesised organic-inorganic hybrid materials with fatty alcohol cores and polyacrylate shells. The polymerization process and encapsulation efficiency of the materials were studied, which indicated that the materials have well energy storage application potential. Li et al. [14] prepared a core-shell fluorinated polyacrylate emulsion with acrylic acid and dodecafluoroheptyl methacrylate. They studied the effect of acrylic acid on the conversion rate, stability, particle size and crosslinking. Ting et al. [15] synthesised a self-crosslinking core-shell structure fluoropolyacrylate emulsion with acrylic acid monomer, dodecafluoroheptyl methacrylate and γ-trisethoxypropane silane. The thermal stability and hydrophobic properties of film were greatly improved with a small amount of silicon-containing monomer adding. The film can be used for functional protective coatings such as moisture proof, ice proof and anti-corrosion.

In the study reported here, a core-shell fluorine-silicon modified polyacrylic were prepared with methyl methacrylate (MMA), butyl acrylate (BA), acrylic acid (AA), dodecafluoroheptyl methacrylate (DFMA) and vinyl triethoxysilane (VTEO). Not only that, tetraethyl orthosilicate (TEOS) was introduced to the system to improve the thermal stability and surface performance. TEOS was hydrolyzed to form silica sol, and moderate amount of TEOS led to SiO_2 and VTEO-containing polymeric segment with chemical bond, which had more excellent in dispersibility and stability. Even if the content of TEOS was excessively added, the resulting silica sol could be miscible with the polyacrylate emulsion in any ratio. Through we chose a ratio of 1:1 for VTEO-TEOS with a literature survey of TEOS applications[16]. As the research on the preparation process of core-shell emulsion, we didn’t discuss the influence of monomer ratio, initiator and emulsifier on the emulsion performance during the polymerization process. The key analysis of the relevant properties was corrosion protection and related aspects. The performance of coating was analysed with electrochemical testing, surface performance and long-term immersion experiments.

2. MATERIALS AND METHOD

2.1 Materials

Methyl methacrylate (MMA), butyl acrylate (BA), acrylic acid (AA), tetraethyl orthosilicate (TEOS), sodium dodecyl sulfate (SDS), OP-10, and ammonium persulfate (APS) were purchased in Chengdu Cologne Chemical Co, Ltd. Dodecafluoroheptyl methacrylate (DFMA) was from UPF technology, and vinyl triethoxysilane (VTEO) was from Aladdin. We used deionized water throughout the process.

2.2 Preparation

The emulsifiers were compounded with SDS and OP-10, mixed in deionized water at 50℃ to prepare an emulsifier solution with the ratio of 2:1. Initiator APS was mixed with deionized water into an initiator solution. A polyacrylic acid monomer containing no-modifier was used to the core-layer, mixed in an emulsifier water solution to form a pre-emulsion I, and the fluorine modifier monomer and the acrylic monomer were mixed and prepared pre-emulsion II with emulsifier solution.

First, polymerization of the core emulsion was carried out in a four-necked flask equipped with a mechanical stirrer, a constant pressure separatory funnel, a condenser and a thermometer. The pre-emulsion I and the initiator were added at 75℃, when the emulsion started to bluish, the core-layer monomer pre-emulsion II was added. The temperature was increased to 85°C and VTEO was added and reacted for 1 hour. Then, the temperature was lowered to 55°C and TEOS was added and reacted for 12 hours. Finally, adjusted the pH of the emulsion to pH 8-9.

2.3 Surface preparation of stainless steel 304

The corrosion substrate was made of stainless steel 304 with a size of 40 mm×13 mm×2 mm. Polish with emery paper of different grades (400, 600, 800 and 1200), cleaned with acetone and rinsed with distilled water, dried in the air and desiccators prior before use. The film was coated with a wire bar coater to control the size 50~60 μm of the film thickness, dried and solidified in the oven at 60℃ for 12 h. For convenience of comparison, we marked the sample without silicon monomer as F-PA , the sample with silicon monomer as F-Si-PA. The silicon monomer was also named VTEO-TEOS, and the samples according to different silicon contents(0.5%、1.0%、1.5%、2.0%) were labeled as F-0.5Si, F-1.0Si, F-1.5Si and F-2.0Si.

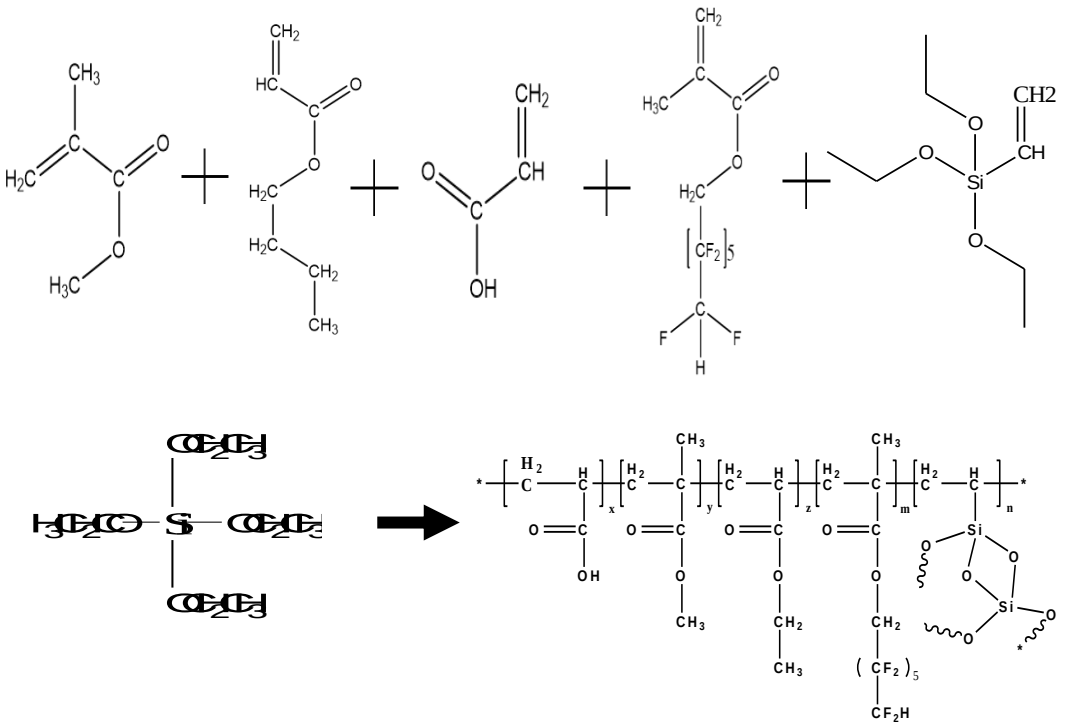

Scheme 1. Schematic diagram of fluorine-silicon modified polyacrylate reaction

2.4 Characterizations

The composition of the emulsion was analyzed using FT-IR spectra in the wavenumber ranges from 500 cm^{-1} to 4000 cm^{-1} with a resolution of 4 cm^{-1}.

Thermogravimetry (TGA) of the copolymer was characterized on a SDTA85 Mettler-Toledo Switzerland. The temperature was ranging from 50 to 500℃ at a heating rate of 10℃/min with N_2 protection. Glass transition temperature was recorded on a differential scanning calorimetry (DSC) instrument at a heating rate of 5℃/min from 0 to 200℃.

The water content angle of the film surface was measured by TBU95 Dataphysics Instruments GmbH. The experimental result was the average of three tests.

The sample was coated with paraffin, and the working electrode area was 1cm × 1cm. The experimental instrument used an electrochemical workstation from Wuhan Corrtest Instraments. The experiment was carried out at 25℃, the electrolyte solution was 3.5% NaCl solution. The coated stainless steel was the working electrode, the platinum electrode was the auxiliary electrode, and the saturated calomel electrode was the reference electrode. A sine wave with a voltage amplitude of 20 mV was applied during the electrochemical AC impedance measurement, and the frequency was between 10^{-2} and 10^5 Hz. The polarization curves were obtained with a potential scan rate of 0.5 $mV \cdot s^{-1}$. EIS measurements were performed at corrosion potential (E_{ocp}) with amplitude of 5 mV over frequency range of 100 kHz–0.05 Hz.

A ZEISS EV0 MA15 scanning electron microscope (SEM) was used to analyze and observe the surface corrosion morphologies of composite coating samples that had been soaked in a 3.5% NaCl solution. The image magnification was 5 k and the acceleration voltage was 20 kV.

The structure of fluorine-silicone latex particles in acrylic emulsion was observed by transmission electron microscope(TEM, Tecnai G2 F20 S-TWIN).

3. RESULTS AND DISCUSSION

3.1 FT-IR and surface analysis

FT-IR spectra of F-PA and F-Si-PA were shown in Fig. 1. The characteristic stretching vibration peak of C-O appears at 1733 cm^{-1}, and the $-CH_3$, $-CH_2$ groups appears at 2955cm^{-1}. The appearance of these peaks indicates the presence of polyacrylate structures in the film [17, 18].At peak of 1238cm^{-1} and 1162 cm^{-1} was characteristic of C-F, which proved the successful introduction of a fluorine-containing monomer in the film [19, 20]. Compared with the F-PA sample, the F-Si sample showed a sharp infrared absorption peaks at 600 cm^{-1}, which proved the existence of Si-O-C [17, 21].There were no obvious C=C and Si-OH absorption peaks in the system, which proves that the system reaction was relatively complete.

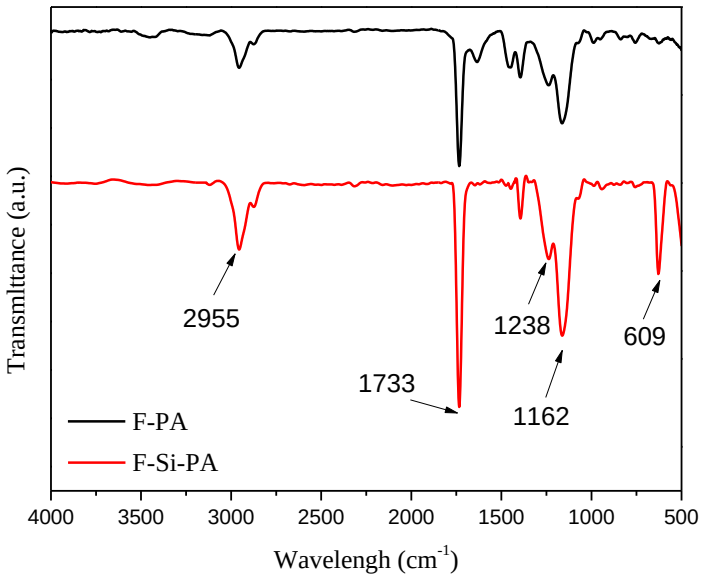

Figure 1. FT-IR spectra of fluorinated polyacrylic and fluorine-silicon Polyacrylic

The morphology of the latex particles was shown in Fig. 2A. It could be seen from the figure that the spherical core (dark)-shell (light) structure of the latex particle had a diameter about 150 nm and a shell thickness about 10 nm. The reason for this structure formation was the segmental polymerization between two phases with different properties [22, 23].The network around the latex particles was crosslinked SiO_2 particles, which were formed by hydrolysis of TEOS. The coating's surface morphology was shown in Fig. 2, which showed different contents of silicon monomer that marked F-PA (B), F-1.0Si (C), F-2.0Si (D). The figure indicated that compared with sample F-PA some small bright spot appeared on the surface of sample F-1.0Si. This was SiO_2 particles produced by TEOS hydrolysis. It could also be seen that the high integrity surface was covered uniform distribution with it. The sample F-2.0Si appeared some block defects, the bright spots of surface became more obvious and larger also. This was due to the excessive addition of TEOS, which caused excessive agglomeration of SiO_2. Excessive SiO_2 accumulated on the surface destroyed integrity of the surface.

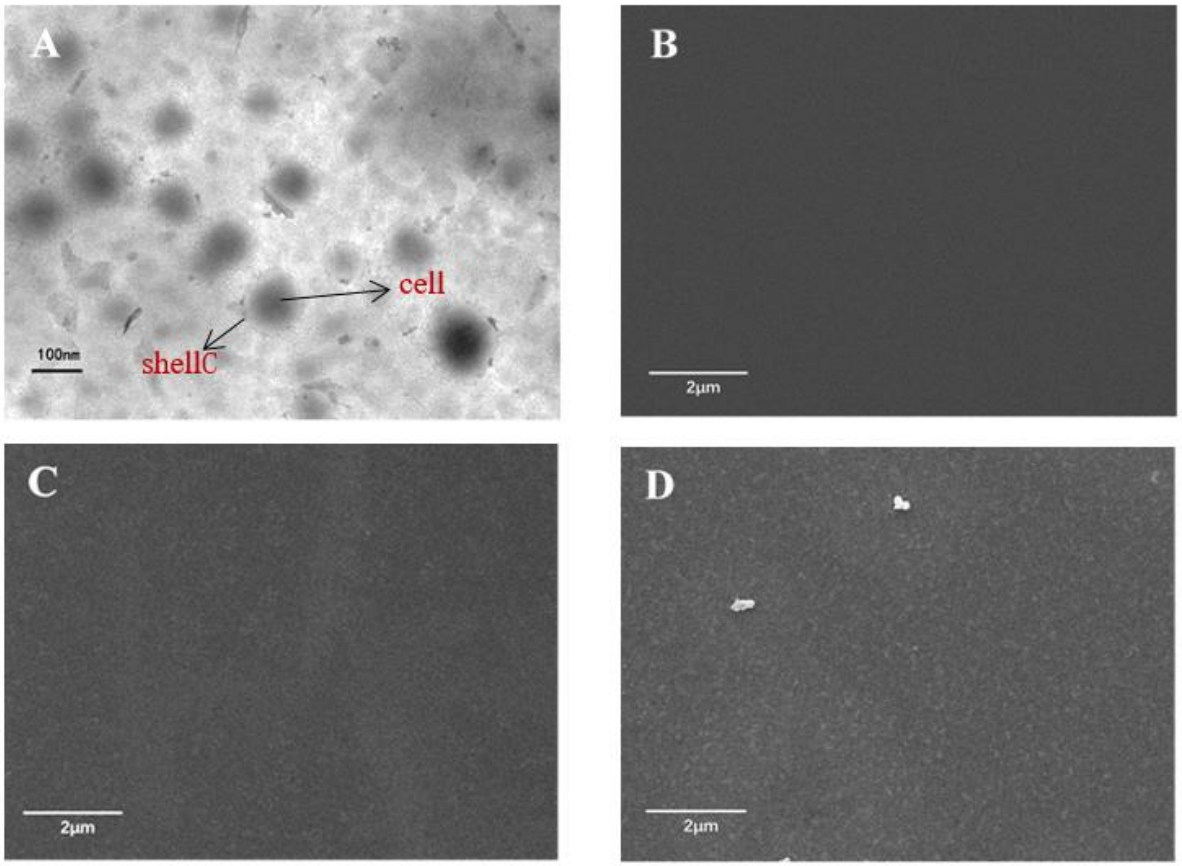

Figure 2. TEM of sample F-1.0Si(A) and SEM of sample F-PA (B), F-1.0Si (C) and F-2.0Si (D)

3.2 Mechanism of corrosion resistance

3.2.1 EIS measurements

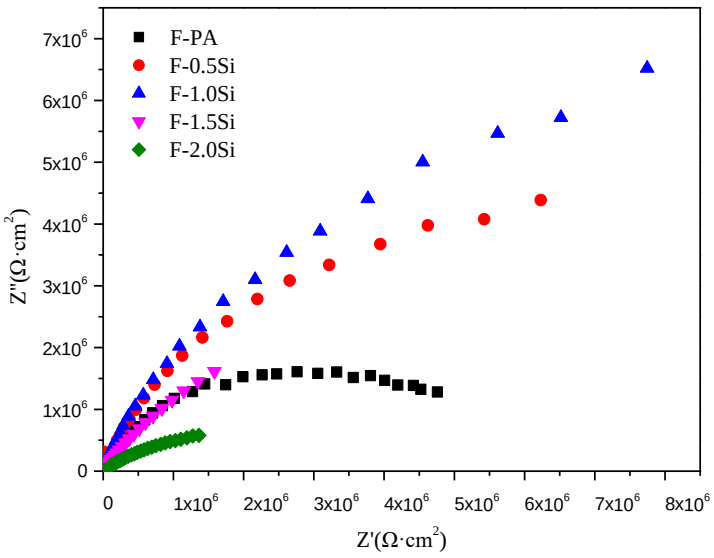

Figure 3. (a) Nyquist plots of coatings with different silicon content in 3.5% NaCl solution

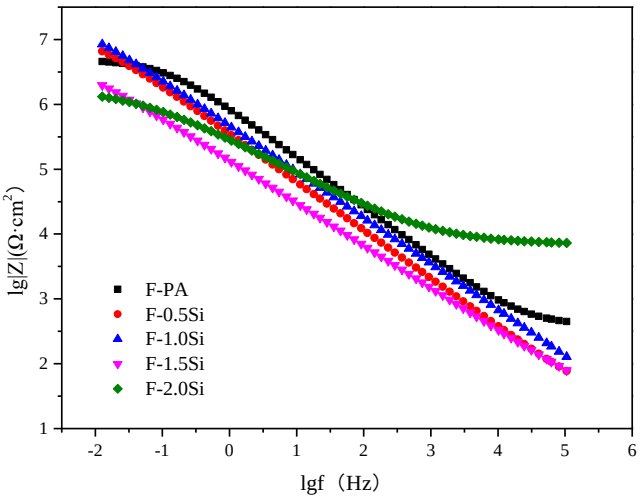

Figure 3. (b) Bode plots of coatings with different silicon content in 3.5% NaCl solution

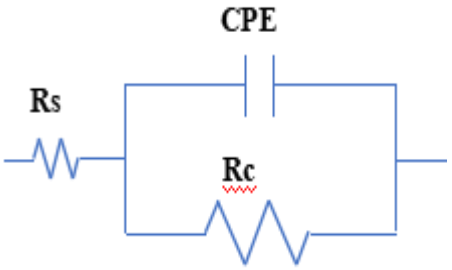

Figure 4. Equivalent circuit diagram of coatings

Table 1. Rs and Rc data for coatings with various VTEO-TEOS contents

Sample	R_s ($\Omega \cdot cm^2$)	CPE		R_c ($\Omega \cdot cm^2$)
		Y_o ($\Omega^{-1} \cdot S^n cm^{-2}$)	n	
F-PA	121.61	5.00×10^{-6}	0.75	2.75×10^{6}
F-0.5Si	151.81	1.73×10^{-6}	0.72	6.32×10^{6}
F-1.0Si	113.24	1.45×10^{-6}	0.81	7.73×10^{6}
F-1.5Si	111.01	1.83×10^{-6}	0.76	1.67×10^{6}
F-2.0Si	109.35	2.06×10^{-6}	0.68	1.43×10^{6}

A series of emulsions with different silicon monomer content were prepared by core-shell emulsion polymerization. The effect of VTEO-TEOS content on corrosion protection performance of film was studied by EIS. The impedance spectrum obtained after immersion for 4 hours was shown in Fig. 3. The impedance arc of sample F-0.5Si and F-1.0Si were higher than the sample F-PA's, which indicated that the addition of some amount of VTEO-TEOS helped to improve the anti-corrosion

performance of the film. As the content continued to increase, the impedance arc began to decrease on the contrary. Just as samples F-1.5Si and F-2.0Si were lower than F-1.0Si, it showed that as the content of VTEO-TEOS increases, the corrosion resistance decreases. The best group of samples was F-1.0Si, the content of VTEO was 1.0g with 3.0% of total monomer.

The impedance data was fitted based on the equivalent circuit model shown in Figure 4. The impedance fitting parameters are shown in Table 1. In the figure, R_s represents the resistance of the solution, CPE was constant phase elements representing the coating and R_c was the coating resistance. The fitted data showed that the introduction of VTEO-TEOS as a filler greatly increases the coating resistance of the composite coating. When the addition amount of VTEO-TEOS was 0.5%, the capacitance value of the composite coating was small, and the maximum resistance value was $7.73\times10^6\Omega\cdot cm^2$. It was 200% higher than the coating without adding silicon monomer.

Corrosion current density (I_{corr}) and corrosion potential (E_{corr}) could indicate changes in corrosion rate and tendency [24] .The smaller I_{corr} was, the corrosion rate lower, and the higher E_{corr} expressed the less corrosion tendency to occur[25] .The same sample was tested for polarization curves ad shown in Fig. 5. Compared with the polarization curve of the sample F-PA, the spectra of sample F-0.5Si and F-1.0Si were moved to the lower right. Which indicates the lower Icorr and higher E_{corr}. At the same with EIS, the performance of sample F-1.5Si and F-2.0Si were decrease, the spectra of them were moved to upper left. Table 2 showed parameter of the fitting obtained polarization curves with software. The protection efficiency of film could be calculated by the following formula [26]:

$$\eta\% = \frac{I_{bare} - I_{corr}}{I_{bare}} \times 100\%$$

The same conclusion as EIS, the sample F-1.0Si had the best performance.When the amount of VTEO-TEOS added was 0.5%, the maximum corrosion potential of the composite coating was -0.182 V and the minimum self-corrosion current density was 5.04×10^{-8} $A\cdot cm^{-2}$. This is two orders of magnitude lower than that of a pure coating. Our EIS test proved that the 0.5% VTEO-TEOS coating has a corrosion inhibition efficiency of 99.53% and excellent corrosion resistance.

Table 2. Tafel polarization curve parameters of bare steel and other samples

Sample	F-PA	F-0.5Si	F-1.0Si	F-1.5Si	F-2.0Si	Bare
I_{corr} (μA)	0.361	0.0504	0.0370	0.671	3.14	7.962
E_{corr} (V)	-0.218	-0.182	-0.150	-0.344	-0.372	-0.518
η (%)	95.46	99.36	99.53	91.57	60.56	——

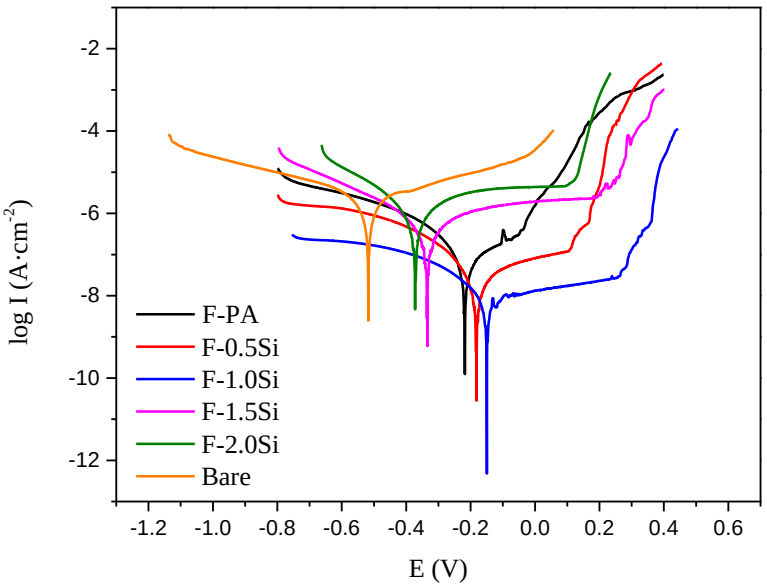

Figure 5. Polarization curves of coatings with various VTEO-TEOS contents after immersion in a 3.5% NaCl solution for 12h

The reason for this phenomenon could be seen from the surface topography of SEM. As a silane coupling, VTEO increased the performance of emulsion's crosslinking and density, so the barrier effect of film was enhanced. The hydrolysis of TEOS made the presence of SiO_2 in the system, which was connected to the polymer segment with chemical bonds and filled some small defects of the film, also increased the barrier effect. The effect of VTEO-TEOS on the properties of film was less, when the content low. So that the properties of film increased with the content. It would caused its own hydrolysis and condensation to form vinyl triol polycondensate when the content was overdose. The viscosity of system was increased, had a negative impact for the stability of emulsion and integrity of the film. The protection performance declined after excessive addition of VTEO-TEOS. Although the excessive amount of TEOS hydrolyzed silica sol could be miscible with the polyacrylate emulsion in any ratio, the too high SiO_2 content would have negative impact on film integrity. As shown in Fig. 2D, the film became no longer smooth after adding excessive silicon monomer, and SiO_2 began to agglomerate, resulting in a decrease in the protective performance of the coating. The protection efficiency of the F-2.0Si sample was only 60.56%, it was even far lower than the protection efficiency before the addition of silicon monomer.

3.2.2 Surface properties

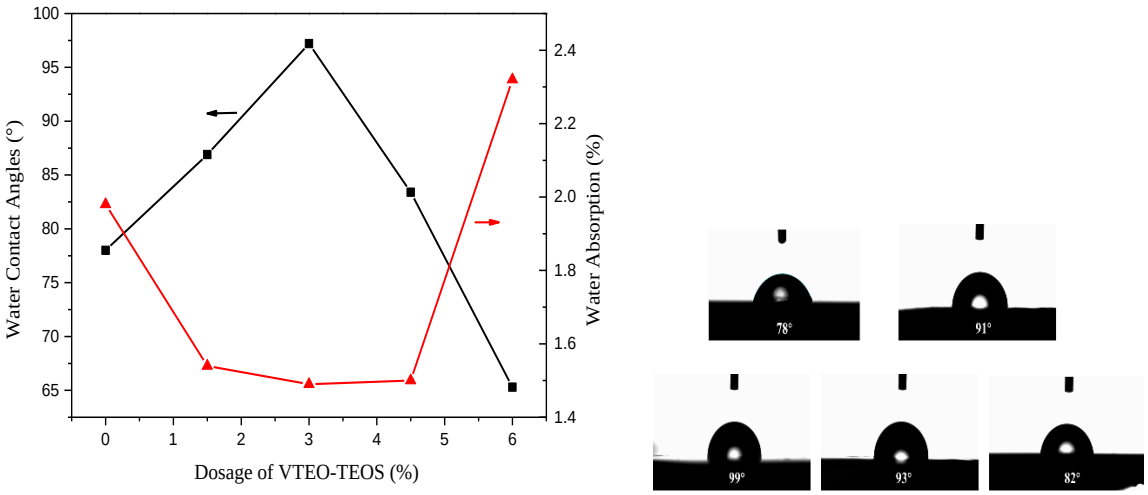

Figure 6. Water contact angle and water absorption of different content of VTEO-TEOS

From the above conclusions, the change of film surface performance could be inferred, it should be modified in the same way as the change of corrosion protection performance. The decrease of surface energy made the change of water contact angle on the surface of the film. The lower surface energy was, the larger static contact angle of water then. The stronger water repellency made the protection of the film better [27, 28] .The quality of film could increase due to the penetration of water during the soaking process. So that the strength of film could be evaluated by increasing in the mass of film at the same soaking time. The surface water contact angle and water absorption of the five different VTEO-TEOS sample were shown in Fig. 6. From the figure it could be seen that the contact angle and water absorption rate shown the same regularity. With the increase of VTEO-TEOS content, the protective performance of film increased first and then decreased. The water contact angle of the sample F-PA was 78°. The surface energy of film was further reduced with the addition of VTEO-TEOS. The water contact angle increased to over 90°, the highest angle was 99° in the surface of sample F-1.0Si. The excess VTEO-TEOS content not only destroyed the integrity of the film, but also reduced the specific gravity of the fluorine on the film surface. That resulted the water contact angle decreased, the water repellency lower and the water absorption rate improved. Based on the above analysis, we found that the performance of sample F-1.0Si was the best.

3.3 Thermal properties

The silicon monomers addition not only effected on the surface performance of film, but also improved the thermal properties [29, 30] .Fig. 7 shown a comparison of thermogravimetric cures of the sample F-1.0Si and the unadded silicon monomer F-PA. Compared with F-PA, the thermal decomposition temperature of F-1.0Si was increased by 16°C. The C-F bond had well thermal stability and could also protected other molecular segments. The sample F-PA had a high thermal

decomposition temperature 282℃, the higher performance of sample F-1.0Si was because of Si-O-Si bond also had well thermal stability, the thermal decomposition temperature was 298℃. The higher residual amount could also be seen F-1.0Si than F-PA, which was due to the presence of SiO_2 in the F-1.0Si system [31, 32] .

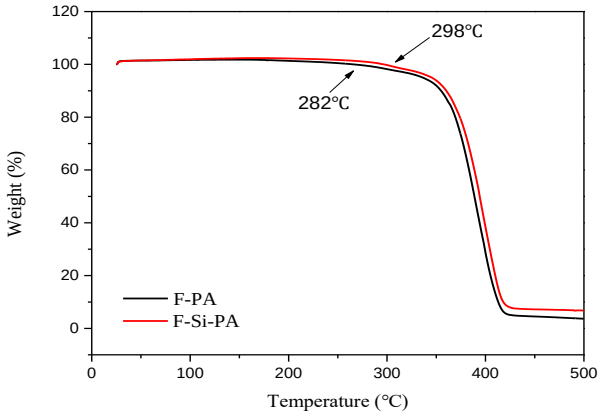

Figure 7. Thermogravimetric curves of sample F-PA and F-1.0Si

3.4 Long-term immersion

The Fig. 8 was shown that the EIS of sample F-1.0Si for long-term immersion. Fitting data with circuit diagram in Fig. 8, the parameters were given in Table 2. In the early stage of immersion, the sample exhibited a high-impedance, low-capacitance and high-efficiency barrier layer with an impedance value of $10^8\Omega\cdot cm^2$ or more. With the increase of immersion time, water molecules began to penetrate the coating, corrosive ions also invaded, and the substrate started to corrode [33]. After 96 h immersion, the film protective performance decreased, but it was still well. The impedance arc of immersion exceeding 312h was close to the bare steel, the protective performance was almost disappeared. In the fitting circuit diagram, Rs was the solution resistance, which was much smaller than the film resistance, so it could be ignored. Rt represented the charge transfer resistance, indicating the ease which the corrosion medium reacted with the metal. Rc represented the film resistance. It could be seen from the fitting parameter table that the resistance of substrate to corrosion medium mainly was acted on the film resistance and the charge transfer resistance. The charge transfer resistance was derived from the resistance of the coated substrate system to corrosion media, which was around $10^6\ \Omega\cdot cm^2$. The film resistance was $2.08\times10^8\Omega\cdot cm^2$ at the initial stage of immersion, and the resistance gradually decreased with the increase of the soaking time. The resistance of the film after immersion for more than 48 hours had a nearly one-order decrease, but it still had a well protective effect, and the impedance was above $10^7\Omega\cdot cm^2$. The film resistance property with the immersion time exceeding 312 h decreased significantly, the film began to fail, the impedance fell below $10^5\Omega\cdot cm^2$. The change in the resistance of the film was related to the degree of diffusion of water. By fitting the capacitance data, the volume fraction of water in the coating could be calculated [34, 35]:

$$\varphi = \frac{\log(C_t/C_0)}{\log 80}$$

C_t represented the film capacitance at time t, C_0 represented the initial film capacitance. The calculated result was shown in Fig. 9. The diffusion of water in the film during the immersion process could be divided into three stages, a continuous growth stage in the initial stage of immersion, a slow growth stage in the middle stage and a stable stage in the late. The continuous growth phase in the initial stage of immersion corresponded to the high-impedance part of the impedance spectrum. Due to the short immersion time, the film was complete and less volume fraction of water, so that it had better protection performance. As time increased, the volume fraction of water in the film tended to be saturated, so the volume fraction change of the water began to slow down. But it also provided more diffusion channels for the corrosive medium, which led the protective performance of the coating to decline in the middle of immersion. When the water molecules were supersaturated, the immersion of water began to decrease the adhesion between film and substrate. Finally, water molecules fill between the substrate and the coating, so there was a stable stage of the volume fraction of water in the coating at the later stage of immersion and the protective performance of the coating almost disappeared .

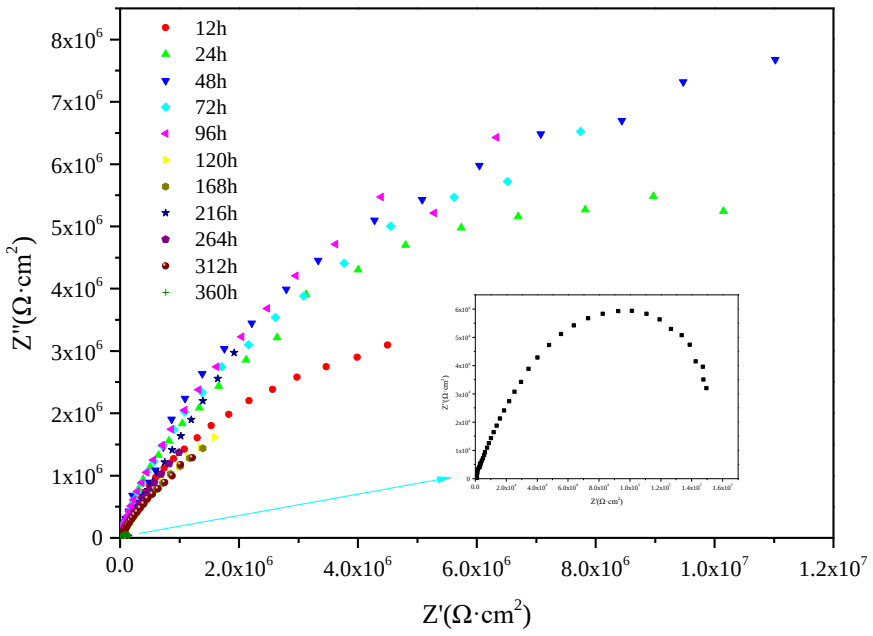

Figure 8. (a) Nyquist plots of coatings after immersion in 3.5% NaCl for various time periods

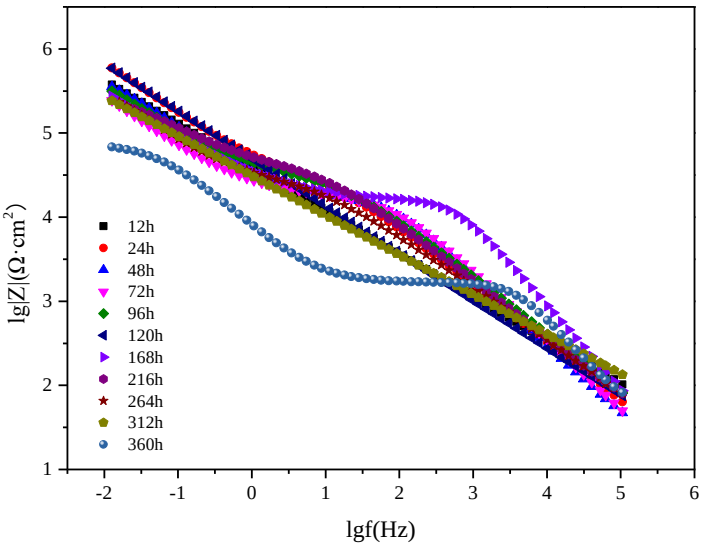

Figure 8. (b) Bode plots of coatings after immersion in 3.5% NaCl for various time periods

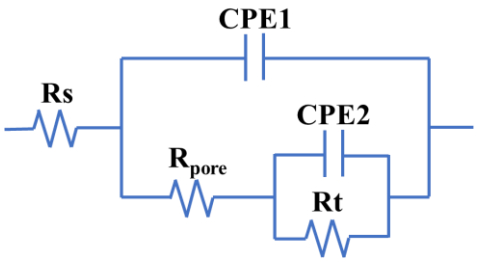

Figure 9. Fitting circuit diagram

Table 3. Rs, Rc, and Rt for coatings with various immersion time as determined via Nyquist plot fitting

Time(h)	Rs ($\Omega \cdot cm^2$)	CPE1 ($\Omega^{-1} \cdot S^n cm^{-2}$)	Rc ($\Omega \cdot cm^2$)	CPE2 ($\Omega^{-1} \cdot S^n cm^{-2}$)	Rt ($\Omega \cdot cm^2$)
12	332.23	1.45×10^{-8}	2.08×10^{8}	9.75×10^{-7}	1.98×10^{6}
48	351.38	3.25×10^{-7}	1.53×10^{6}	4.94×10^{-8}	1.89×10^{6}
96	328.82	5.70×10^{-7}	2.56×10^{6}	1.20×10^{-7}	1.80×10^{6}
120	358.59	3.18×10^{-7}	1.25×10^{5}	1.99×10^{-6}	7.04×10^{6}
168	355.89	1.49×10^{-6}	3.94×10^{4}	1.28×10^{-6}	5.54×10^{6}
312	360.51	1.84×10^{-5}	7.24×10^{3}	2.23×10^{-7}	9.80×10^{5}
360	343.98	1.88×10^{-5}	5.09×10^{3}	1.07×10^{-7}	2.15×10^{5}

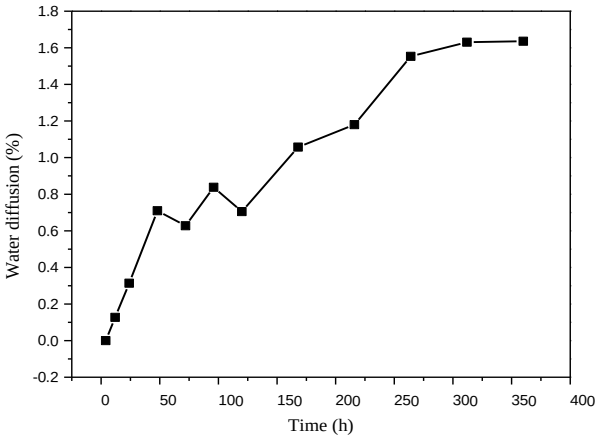

Figure 10. Diffusion of water in film at different immersion time

3.5 Mechanism

As an insulating layer, the organic coating was generally considered to have a barrier mechanism and a bonding mechanism. Since the emulsion in the paper was a special core-shell structure of existence fluorine and silicon monomer, the analysis of the corrosion protection mechanism of the film could begin from the film formation process of the structure. Zhong [36] et al. synthesized a fluorine-containing acrylate-siloxane modified water-based alkyd hybrid resin using a microemulsion polymerization process. Its latex particles were also core-shell structure. The electrochemical corrosion studies revealed that the cross-linked coating exhibited superior corrosion resistance performance with an inhibition efficiency of 99.95% and a corrosion rate of 6.95×10^{-3} mm per year.

The film formation process was shown in scheme 2, when different diameters particle was present in the system, small size particles could be effectively filled in the voids of the large, and the packing efficiency of the latex particles was improved. Since the voids extended to the surface of the film, if the total number of integrals of the small particles was sufficiently high, the voids between the large particles could be completely filled and enriched in the surface of the film. Due to the enrichment effect the fluorine-containing segment was concentrated on the surface of the film, and the size effect made the small-sized SiO_2 fills defects, which greatly promotes the performance of the film surface. It also explained the improvement of the hydrophobic properties and the corrosion resistance of the film surface when the amount of VTEO-TEOS was small. When the content was too much, the hydrolysis of VTEO and the excess of SiO_2 would affect the integrity of the film, so there was the phenomenon that the film performance of VTEO-TEOS addition was not as well as the sample without addition. It could be seen from the immersion time experiment that the effective time of the film was only within 300h, which might be related to the adhesion of the film. With the intrusion of water molecules, not only the defects in the coating will increase, but also the adhesion will decrease. Due to the bonding mechanism, the coated metal system maintained a high resistance to corrosion ions. When the coating adhesion decreases, the resistance of the system to corrosion ions was weakened, and corrosion was

more likely to occur. The decrease in adhesion would also reduce the barrier effect of the coating, so once the coating performance begins to decrease, the failure would occur quickly.

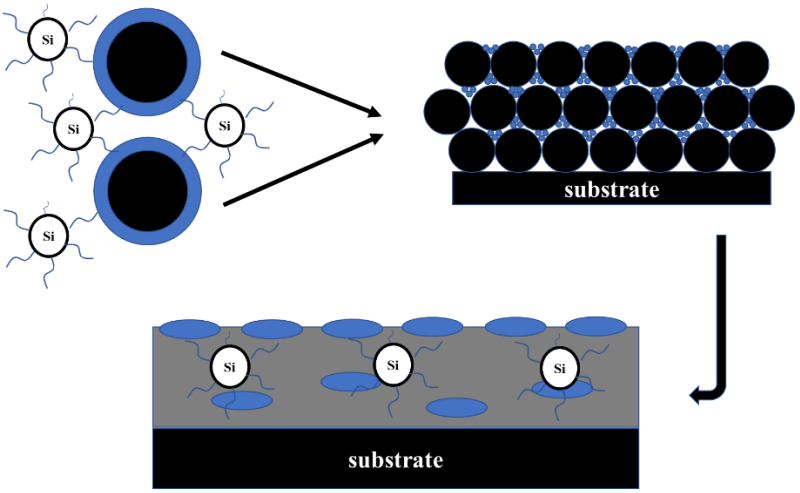

Scheme 2. Sketch of film formation process

4. CONCLUSIONS

The fluorine-silicon modified polyacrylate emulsion was prepared by core-shell emulsion polymerization. The FT-IR test showed that the reaction was relatively complete and the fluorine-silicon groups had been added to the polymer chain. TEM showed that the emulsion had a round core-shell structure with different light and dark. Finally, the application of emulsion in corrosion protection coating was studied. Electrochemical tests showed that the impedance of the film could reach above $10^8\ \Omega\cdot cm^2$. The protection performance increased first and then decreased with the addition of silicon monomer content. The polarization resulted calculate the best corrosion protection efficiency of 99.53%. The film after adding silicon monomer had excellent hydrophobicity and water contact angle of up to 99°. The addition of VTEO-TEOS increased the crosslinking performance, stability and hydrophobicity of the system, and thus the overall corrosion protection performance of the film was improved. However, long-term immersion experiments showed that the protective performance of the film could only last for about 300 hours. The duration of the protective effect was short, and it would quickly fail once the performance began to decline. The emulsion needed to be further research for applied large scale in actual production and life.

ACKNOWLEDGEMENTS
This work was supported by the National Natural Science Foundation of China (No.51774242.) and National Natural Science Foundation of China(Research on New Acidification Corrosion Inhibitor Based on Indolizine Derivatives and Its Mechanism, No. 52074339).

References

1. D.Dhanapal , G.Rebheka , S.Palanivel and A.K.Srinivasan, *Surf. Innovations*, 3(2014)127.
2. C.X. Sun, J.J. Dai, H.X. Zhang, F.Y. Zhang and N.Y.Zhang, *Prog. Org. Coat.*, 128(2019)21.
3. X.Wang, L. Hou, L.L. Xu, X. Li, Y. Gu and Q. Zhang, *Int. J. Electrochem. Sci.*, 15 (2020)1450.
4. A. H. El-Shazly and H. A. Al-Turaif, *Int. J. Electrochem. Sci.*, 7(2012)211.
5. A.Fahim , E.Dean , M.A.D.Thomas and E.G.Moffatt, *Mater. Corros.*, 70 (2019)328.
6. J. Liu, C.M. Wang, W.L.Zhang L, T.T. Xia, X.H. Zhang, T.X. Liang, T.Ahmad and H. YANG, *Mater. Sci. Technol*., 35 (2019)907.
7. S.F. Zhang, F.R. Liu, Y.F.He, R.M. Wang, P.F. Song and L.J. Ma, *Arab. J. Sci. Eng*. , 39(2014)23.
8. O.Yilmaz, M.Karesoja, A.C.Adiguzel, G.Zengin and H.Tenhu, *J. Polym. Sci. Pol. Chem*., 52 (2014)1435.
9. O. Yilmaz, *Prog. Org. Coat*. , 127 (2019)266.
10. G.A.Alvarez, Fuensanta, Mónica, Orozco, H.Víctor, Giraldo F.Luis , Martín-Martínez and José Miguel, *Prog. Org. Coat*., 118 (2018)30.
11. C.Xu, J.Ma, G.H. Li , N.Y. Wang, Q.X. Zhang, M.E. Grami and X.W. Qu, *J. Polym. Res.*, 147 (2017)1.
12. X.Y. Zhang, Y.H. Liu, H.Huang,Y.J. Li and H.Q. Chen, *J. Appl. Polym. Sci*., 123 (2012)1822.
13. Batürk, Emre Emre, M.V.Kahraman and V.Memet, *Polym. Eng. Sci.*, 58 (2018)2166.
14. K.Q. Li, X.R. Zeng, H.Q. Li and X.J. Lai, *J. Appl. Polym. Sci*. ,77 (2015)1.
15. T. Lu, D.M. Qi , D. Zhang, Q. Liu and H.T. Zhao , *React. Funct. Polym.*, 104 (2016)9.
16. J.H. Zhou, X. Chen, H. Duan and J.Z. Ma, *Polym. Int.* ,64 (2015)1373.
17. X. Jiang, J. Gu, X.Z. Tian, D. Huan and Y.Q. Yang, *J. Dispersion Sci. Technol.*, 32 (2011)1266.
18. Xu WJ, He QL,Zhang SJ,Zhang WS, *Polym. Bull.*, 75 (2018)1171.
19. W. Xu, Q.F. An, L.F. Hao, Z. Sun and W.J. Zhao, *FIBER POLYM.*, 14 (2013)895.
20. X.J. Cui , Z.X. Chen, Q.S. Li, S.L. Zhong and H.Y. Wang, *J. Appl. Polym. Sci.* ,105 (2007)2138.
21. M.X. Zou, Q.C. Zhao, J. Nie and Z.J. Zhang, *J. Appl. Polym. Sci.* ,103(2007)1406.
22. B.Y. Li, S.J. Zhang, Q. Xu and B. Wang, *Polym. Adv. Technol.* ,20 (2010)1190.
23. J.H. Zhou, Y.J. Cui, L.B. Wang and P.B. Wei, *Polym. Compos.*, 39 (2018)4467.
24. Phanrapee, Suwadee, Pattarapan, Suwadee,Prasassarakich and Pattarapan. *Prog. Org. Coat.* 85 (2015)84.
25. S. Liu, L. Gu, H.C. Zhao and H.B. Yu, *J. Mater. Sci. Technol.* ,32 (2016)425-431.
26. X.K. Cui, G.Y. Zhu, Y.F. Pan, Q. Shao, X.X. Zhao, M.Y. Dong , Y. Zhang and Z.H. Guo, *Polymer.*, 138 (2018)203.
27. G.Christopher and M.A.Kulandainathan, *Prog. Org. Coat.*, 99 2016)99.
28. X. Yuan, Z.F. Yue , Z.Q. Liu, S.F. Wen, L. Li and T. Feng , *J. Coat. Technol. Res.* ,13(2016)123.
29. 29.X. Wang, H. Wang, D.X. Zhang, L. Hou and H. Jiang, *Int. J. Electrochem. Sci.*, 14 (2019)777.
30. L. Lei, H.M. Lou, Y.L. Xiao, G.Z. Zhang, C.Y. Wang and Y.H. Deng, *RSC Adv.*, 8 (2018)4604-4609.
31. X.U. Zhang, Y. Zhong, X.F. Sui, L.P. Hong and Z.P. Mao, *Color. Technol.*, 134 (2018)299.
32. P.P. Chen, Z.H. Cheng, F.X. Chu, Y.Z. Xu and C.P. Wang, *J. Nanopart. Res.* ,18 (2016)124.
33. Y. He, C.L. Chen, G.Q. Xiao, F. Zhong, Y.Q. Wu and Z. He, *React. Funct. Polym.*, 137 (2019)104.
34. Y.N. Zhang, Q.H. Fang,J.S. Chen and N.J. Wang, *Prog. Org. Coat.*, 109 (2017)126.
35. J. Li, L.C. Gan, Y.C. Liu, S.Mateti, W.W. Lei, Y. Chen and J.H. Yang, *Eur. Polym. J.*, 104 (2018)57.
36. S.J. Zhong, J.W. Li, L.M. Yi, Y. Cai and W.L. Zhou, *Polym. Adv. Technol.*, 30(2019)292.